Complementary barrier infrared detector (CBIRD) with double tunnel junction contact and quantum dot barrier infrared detector (QD-BIRD)

David Z.-Y. Ting*, Alexander Soibel, Arezou Khoshakhlagh, Sam A. Keo,
Jean Nguyen, Linda Höglund, Jason M. Mumolo, John K. Liu,
Sir B. Rafol, Cory J. Hill, and Sarath D. Gunapala

Center for Infrared Sensors, Jet Propulsion Laboratory,
California Institute of Technology, Pasadena, CA 91109 USA

ABSTRACT

The InAs/GaSb type-II superlattice based complementary barrier infrared detector (CBIRD) has already demonstrated very good performance in long-wavelength infrared (LWIR) detection. In this work, we describe results on a modified CBIRD device that incorporates a double tunnel junction contact designed for robust device and focal plane array processing. The new device also exhibited reduced turn-on voltage. We also report results on the quantum dot barrier infrared detector (QD-BIRD). By incorporating self-assembled InSb quantum dots into the InAsSb absorber of the standard nBn detector structure, the QD-BIRD extend the detector cutoff wavelength from ~4.2 μm to 6 μm, allowing the coverage of the mid-wavelength infrared (MWIR) transmission window. The device has been observed to show infrared response at 225 K.

PACS (2010) Numbers: 78.67.Pt, 85.60.Gz
Keywords: infrared detector, antimonide, type-II superlattice, quantum dot, unipolar barrier
***Corresponding author**: Jet Propulsion Laboratory, M/S 302-231, 4800 Oak Grove Drive,
Pasadena, CA 91109-8099, USA; Ph: +1.818.354.1549; FAX: +1.818.393.4663;
David.Z.Ting@jpl.nasa.gov (D. Z.-Y. Ting)

1. Introduction

The antimonide material system consisting of the nearly lattice-matched semiconductors of InAs, GaSb, and AlSb (and their alloys with InSb, GaAs, and AlAs) has emerged recently as a highly effective platform for the development of sophisticated heterostructure-based mid-wavelength infrared (MWIR) and long-wavelength infrared (LWIR) detectors, as exemplified by the high-performance double heterstructure (DH) [1], nBn [2,3,4], XBn [5,6,7,8], and type-II superlattice infrared detectors [9,10,11,12,13,14,15,16,17,]. A key enabling design element is the unipolar barrier [17], which is used to implement the barrier infra-red detector (BIRD) design for increasing the collection efficiency of photo-generated carriers, and reducing dark current generation without impeding photocurrent flow. In this paper, we report an LWIR antimonide superlattice detector based on the complementary barrier infrared detector (CBIRD) [17] with a modified design, as well as an MWIR quantum dot barrier infrared detector (QD-BIRD) [18] that extends the cutoff wavelength of the standard nBn detector [2].

2. Complementary barrier infrared detector (CBIRD)

The active region of the complementary barrier infrared detector (CBIRD) [17] design consists of a p-type InAs/GaSb long wavelength infrared (LWIR) absorber SL sandwiched between an n-type InAs/AlSb hole-barrier (hB) SL (which also serves as the top contact) and a p-type InAs/GaSb electron-barrier (eB) SL. The hB SL and the eB SL are respectively designed to have approximately zero conduction and valence subband offset with respect to the absorber SL, i.e., they acts as a pair of complementary unipolar barriers with respect to the absorber SL. Underneath the active region is a ~1μm thick highly n-doped InAsSb bottom contact region,

which is connected to the eB SL via a broken-gap tunnel junction. The entire structure is grown on GaSb substrate, with an n-type GaSb buffer layer which is not electrically active.

The structure and performance of the original CBIRD device has been documented in detail elsewhere [17]. In this paper we address two specific areas of device improvement. First, the original CBIRD design uses a rather thick (~1μm) InAsSb bottom contact for the purpose of providing a large processing window for etching to bottom contact layer. The composition of the InAsSb alloy (~$InAs_{0.91}Sb_{0.09}$) must be carefully controlled so that it remains lattice-matched to the GaSb substrate over the 1μm thickness. The precise composition control can be somewhat challenging for growth since InAsSb is a mixed Group-V alloy. The second issue is that the original CBIRD required ~200 mV biasing before it became fully responsive, even though the CBIRD device was designed to turn on fully at zero bias.

The first issue is addressed in Fig. 1, which shows the energy band diagram of a modified CBIRD design. The hole barrier, absorber, and electron barrier comprising the active region are the same as before. The InAsSb layer now has a reduced width of 0.2 μm (to make it less burdensome for growth), and is doped $n=1\times10^{18}$ cm^{-3} as before. It is grown on a p-type GaSb buffer layer, which serves as the new bottom contact. Note that the p-GaSb contact layer could be grown as thick as desired on GaSb substrate. The bottom panel of Fig. 1 shows the broken gap tunnel junctions between the n-InAsSb and the p-type electron barrier SL, as well as between the n-InAsSb and the p-GaSb bottom contact (hence the name double tunnel junction contact). At both of the interfaces, the doping is high to ensure low junction resistance. To summarize, the double tunnel junction design uses a thick (and easy to grow) GaSb contact layer to offer a large processing window; it provides low-resistance electrical connection between the GaSb contact and the absorber layer through two broken-gap tunnel junctions, and avoids the growth of a thick

InAsSb contact layer. We note that the new CBIRD design differs from the original only in doping profile and in the reduction of the InAsSb layer thickness.

One might question necessity of the double tunnel junction at all. Could we not remove the InAsSb layer, and, for that matter, the electron barrier layer also, and connect the absorber directly to the p-GaSb bottom contact, without going through any tunnel junctions? The challenge with this seemingly simpler approach is that valence band edge of GaSb is approximately 100 meV lower than that of the electron barrier SL (and the absorber SL, whose valence band edge nominally lines up with that of the electron barrier SL). This valence band offset would introduce a blocking barrier to holes traversing from the absorber to the bottom contact.

We next address the issue of CBIRD turn-on bias. If we examine the band diagram in the top panel of Fig. 1, we note that there is no a priori reason why the CBIRD device should not have full response at zero bias. Consider an electron-hole pair photo-generated in the p-type absorber superlattice region while the CBIRD structure is under zero bias. Although electron (minority carrier) could diffuse to either direction, the presence of the deflecting electron barrier serves to ensure that all electrons that do not recombine with majority holes in the absorber would eventually move toward the left, and be swept across the (primary) N-p junction at the hole barrier / absorber interface to be collected at the top contact. By dielectric relaxation, the photo-generated hole would push an excess hole to the electron barrier / InAsSb broken-gap tunnel junction (or, in the case of the new design, the double tunnel junction), which allows the excess hole to traverse freely towards the right electrode even under zero bias.

A possible scenario for why a CBIRD device would require a turn-on voltage is illustrated in Fig. 2. The top panel shows the zero-bias energy band diagram of an N-p heterojunction, which is the hole-barrier/absorber portion of the CBIRD structure. The calculation was performed using heterojunction drift-diffusion simulation [19]. The top panel shows the N-p junction as intended by design, with no conduction band offset between the hole barrier and the absorber. The middle panel shows a similar band diagram for the case where there is a hypothetical 80 meV band offset between the hole barrier and the absorber (hole barrier side being higher). Under zero applied bias, band bending reduces the 80 meV band offset barrier to a triangular barrier of ~38 meV, which would still hinder the flow of electron photocurrent towards the left electrode. The bottom panel shows that an applied reverse bias of 200 mV is required to remove the 38 meV triangular barrier and open up the current flow fully.

Another possible scenario is that, even if there is no conduction band offset between the hole barrier and the absorber, there could still be a small unintended electron barrier if the doping junction is moved into the hole barrier region, instead of coinciding with the metallurgical junction. This again would introduce a current-impeding barrier, which has to be overcome by reverse biasing [20]. Both the conduction band offset induced barrier, and the doping profile induced barrier (or combinations of the two) can be removed by making small adjustments to the device structure, by modifying the doping profile or making small changes to the design of the hole barrier superlattice.

A device structure based on the modified CBIRD design was grown on a 50-mm diameter Te-doped GaSb (100) substrate in a Veeco Applied-Epi Gen III molecular beam epitaxy chamber equipped with valved cracking sources for the Group V Sb2 and As2 fluxes. The absorber of this particular device uses 300-period superlattice. Square mesa photodiodes of

area 200 μm × 200 μm were fabricated using standard optical lithography for responsivity and dark current measurements. The devices were not passivated, nor treated with anti-reflection (AR) coating. Figure 3 shows the top illuminated spectral responsivity of the device measured at 77 K, under 0.1 V bias. The responsivity peaks at ~6.5 μm with a value of 1.7 A/W, and drops off to approximately 1.2 A/W at 5 μm. The long wavelength (50% peak responsivity) cutoff occurs at 10 μm, in good agreement with the 77K photoluminescence spectrum peak. Assuming unity gain, the single-pass peak quantum efficiency is ~33%; estimated peak quantum efficiency for AR coated devices is ~46%.

The inset of Fig. 3 shows the peak responsivity as a function of applied bias at 77 K. In contrast to what was observed in the previously reported CBIRD device [17], the photo-response is almost fully turned on at zero bias, reaching 90% of the plateau value. This shows that the unintended conduction band potential barrier at the N-p junction is almost completed removed. It also shows that the new double tunneling junction bottom contact does not introduce any noticeable added resistance.

Figure 4 shows the measured dark current density as a function of applied bias at 77 K. Under 100 mV bias, the dark current density level is 0.89×10^{-5} A/cm^2. The reverse bias (positive top bias) J-V characteristics appears nearly diffusion-limited, with dark current level increasing only by 65% when the applied bias is increased from 50 mV to 300 mV.

We computed the 300 K background black-body specific detectivity (D^*) from the measured 0.1 V spectral responsivity and dark current at 77K detector operating temperature, assuming unity gain. The photocurrent is determined from the integrated photo-response in the 8 μm to 10 μm spectral range (the overlap of the atmospheric transmission window and the detector response). For f/2 viewing conditions, the black-body D^* value is 8.86×10^{10} cm-

$Hz^{1/2}$/W under 0.1 V bias. LWIR imaging focal plane array (FPA) results from the new CBIRD design have been reported [21]. The FPA operating at 78K exhibited an NEDT of 18.6 mK with f/2 optics at 300K background.

3. Quantum dot barrier infrared detector (QD-BIRD)

The recent emergence of barrier infrared detectors such as the nBn [2,3] and the XBn [6] have resulted in mid-wave infrared (MWIR) detectors with substantially higher operating temperatures than previously available in III-V semiconductor based MWIR detectors. The nBn/XBn detector uses a unipolar barrier layer sandwiched between the top contact layer and the absorber layer. The unipolar barrier blocks the flow of majority carriers (electrons), but not minority carriers. The barrier photodetector architecture offers advantages of suppressed generation-recombination (G-R) dark current resulting from suppressed Shockley-Read-Hall (SRH) recombination processes [2,3], and reduced surface leakage dark current [9,22,23,24,25]. The initial nBn devices used either an InAs absorber grown on InAs substrate, or lattice-matched InAsSb alloy grown on GaSb substrate, with cutoff wavelengths of ~3.2 μm and ~4 μm, respectively. While these detectors could operate at much higher temperatures than existing MWIR detectors based on InSb, their spectral responses do not cover the full (3 – 5 μm) MWIR atmospheric transmission window. There also have been nBn detectors based on the InAs/GaSb type-II superlattice (T2SL) absorber that have provided spectral coverage out to longer cutoff wavelengths [11,26]. Here we describe an alternative approach to extending the cutoff wavelength of the standard nBn detector by insert quantum dots into the absorber layer of the nBn.

Figure 5 schematically illustrates the structure of the quantum dot barrier infrared detector (QD-BIRD). It is very similar to the standard nBn device structure as originally described by Maimon and Wicks [2,3], consisting of an AlSbAs barrier sandwiched between the InAsSb top contact layer and absorber layer. The slight modification we introduced is the periodic insertion of 2.8 monolayers (MLs) of InSb, which forms self-assembled InSb quantum dot layers in the InAsSb absorber matrix, as illustrated in Fig. 5. The alloy composition of the InAsSb matrix was adjusted slightly to reduce the Sb content. More details of the structure have been reported earlier [18].

The top panel of Fig. 6 shows the normalized photoluminescence (PL) spectrum of the QD-BIRD with two distinct peaks. The origins of the 4.0 μm and the 5.5 μm peaks are illustrated in Fig. 7, which shows a schematic energy band diagram for the vicinity of the InSb quantum dot. The 4.0 μm peak is easily identified with the band gap E_g of the InAsSb matrix. The 5.5 μm peak is related to the quantum dot. The band diagram shows that the strained InSb forms a type-II broken gap band alignment with the InAsSb matrix, with the valence band edge of InSb being substantially higher than the conduction band edge of InAsSb. The InSb quantum conduction band state is clearly unconfined and is not likely a source of the PL peak. What is most likely responsible for the 5.5 μm PL peak is a type-II transition involving the conduction band edge of the InAsSb matrix, and the confined hole state of the InSb quantum dot, illustrated in Fig. 7 with the label E_{md}.

The bottom panel of Fig. 6 shows the spectral responsivity for a QD-BIRD device, without AR coating, taken at 125K, 175K, and 225K under -200 mV bias. The spectral responsivity is measured using a top-illuminated geometry. Because the GaSb substrate is essentially transparent to the MWIR radiation under consideration, the spectral response should be considered as a double-pass (or multiple-pass) result, since light could re-enter the absorber

region after reflecting off the bottom of the substrate. Like the PL spectrum, the spectral responsivity also shows a distinct bimodal behavior. The photo-response associated with the direct band-to-band transition in the InAsSb matrix is seen at the short wavelengths. The responsivity drops off to 50% of the peak value at 4.22, 4.34, and 4.51 μm at T=125K, 175K, and 225K, respectively. Beyond the cutoff wavelength associated with the bulk InAsSb matrix, we also observe extended response which drops off approximately linearly; this is attributed to the type-II transition between the quantum dot valence band state and the InAsSb matrix conduction band state. The extended response associated with the quantum dots is noticeably weaker than the bulk InAsSb response. The external quantum efficiencies at 5 μm for T=125K, 175K, and 225K are respectively 8.6%, 16%, and 17.5%, which are only about 30% the corresponding values found for the InAsSb matrix in the 3-4 μm range, even though the PL intensities of the QD-to-matrix and the bulk transitions are comparable. One reason for the weaker response of the QD-to-matrix transition is that the quantum dot hole state is confined by the InAsSb matrix. The confinement energy ΔE is given by the difference between the InAsSb band gap E_g and the QD-to-matrix transition energy E_{md} (see Fig. 7). The photo-excited hole (minority carrier) has to overcome this additional energy barrier ΔE in order to escape the quantum dot and be collected. There is likely a distribution of quantum dot sizes, with a corresponding distribution E_{md} and ΔE. Smaller dots that lead to longer the extended wavelength (smaller E_{md}) would have larger escape energy ΔE. This would explain why the extended cutoff response tails off as the wavelength increases.

The bottom panel of Fig. 6 shows that the photo-response increases with temperature; the responsivity at 225K is approximately twice that at 125K. One possible mechanism responsible for this behavior is the presence of a small un-intended hole barrier resulting from the valence band mismatch between the absorber and the AlSbAs barrier (the valence band edges of the

absorber and the barrier should be aligned in an ideal nBn structure). This barrier would block photo-currents generated from both the InAsSb matrix absorption and the dot-to-matrix absorption. Another possibility is that the quantum dots themselves could impede minority carrier transport. A QD occupied by a hole is a (screened) Coulomb scattering center, which in principle could provide the observed temperature dependence. An unoccupied QD could also trap holes.

Figure 8 shows the measured dark current density for a QD-BIRD as a function of applied bias at 125K, 175K, and 240K. The reverse-bias (negative top contact bias) J-V characteristics appear diffusion-limited at 17K and 240K. Under -200 mV bias, the dark current density levels are 1.52×10^{-7} A/cm^2 and 3.77×10^{-4} A/cm^2, respectively at 125K and 175K. We computed the black-body specific detectivity (D^*) for f/2 optics, 300 K background conditions.

The photocurrent is determined from the integrated photo-response in the 3 μm to 6 μm spectral range. For detector temperature of T=175K, -200 mV bias, the black-body D^* is dark-current limited and has a value of 1.07×10^{11} cm-Hz$^{1/2}$/W. At T=125K, the black-body D^* is background limited and has a value of 3.76×10^{12} cm-Hz$^{1/2}$/W.

Summary

We describe modified complementary barrier infrared detector (CBIRD) [17] structure with a double tunnel junction contact designed for robust device and focal plane array processing. We analyzed the turn-on characteristics of the original CBIRD, and demonstrated results from a new CBIRD device with near zero-bias turn on and near diffusion-limited dark current characteristics at 77K. We also describe results on the quantum dot barrier infrared detector (QD-BIRD), which is a simple modification of the standard MWIR nBn detector with

an InAsSb absorber lattice-matched to the GaSb substrate. We showed that by incorporating self-assembled InSb quantum dots into the InAsSb absorber matrix, we could extend the detector cutoff wavelength from ~4.2 μm to 6 μm, and thus providing better spectral coverage of the MWIR transmission window.

Acknowledgments

The authors thank S. Bandara, E. R. Blazejewski, D. R. Rhiger, and J. N. Schulman for helpful discussions, and M. Tidrow, R. Liang, M. Herman, E. Kolawa, and P. Dimotakis for encouragement and support. The research described in this publication was carried out at the Jet Propulsion Laboratory, California Institute of Technology, under a contract with the National Aeronautics and Space Administration. Government sponsorship acknowledged.

---

1. M. Carras, J. L. Reverchon, G. Marre, C. Renard, B. Vinter, X. Marcadet, and V. Berger, Interface band gap engineering in InAsSb photodiodes, *Appl. Phys. Lett*. **87**(10) 102103 (2005)

2. S. Maimon and G. W. Wicks, InAsSb/GaAlSb/InAsSb nBn IR detector for the 3-5 μm, Program and Abstracts, 11th International Conference on Narrow Gap Semiconductors, June 16-20, 2003, Buffalo, New York.

3. S. Maimon and G. W. Wicks, nBn detector, an infrared detector with reduced dark current and higher operating temperature, *Appl. Phys. Lett*. **89**(15) 151109 (2006).

4. J. R. Pedrazzani, S. Maimon and G. W. Wicks, Use of nBn structures to suppress surface leakage currents in unpassivated InAs infrared photodetectors, *Electronics Lett*. **44**(25) 1487-1488 (2008).

5. P. Klipstein, Depletion-less photodiode with suppressed dark current and method for producing the same, United States Patent No: US 7,795,640 B2 (Sep 14, 2010)

6. P. Klipstein, "XBn" barrier photodetectors for high sensitivity and high operating temperature infrared sensors, *Proc. of SPIE*. 6940 (2008) 69402U.

7. Olga Klin, Steve Grossman, Noam Snapi, Maya Brumer, Inna Lukomsky, Michael Yassen, Boris Yofis, Alex Glozman, Ami Zemel, Tal Fishman, Eyal Berkowitz, Osnat Magen, Joelle Oiknine-Schlesinger, Itay Shtrichman, Eliezer Weiss and P C Klipstein, Proc. Infrared Technology and Applications XXXV, Progress with antimonide-based detectors at SCD, SPIE 7298, 7298-0G (2009).

8. Philip Klipstein, Olga Klin, Steve Grossman, Noam Snapi, Barak Yaakobovitz, Maya Brumer, Inna Lukomsky, Daniel Aronov, Michael Yassen, Boris Yofis, Alex Glozman, Tal Fishman, Eyal Berkowicz, Osnat Magen, Itay Shtrichman, and Eliezer Weiss, XBn barrier detectors for high operating temperatures, Proc. SPIE 7608, 76081V (2010).

9. F. Fuchs, U. Weimer, W. Pletschen, J. Schmitz, E. Ahlswere, M. Walter, J. Wagner, and P. Koidl, High performance InAs/$Ga_{1-x}In_xSb$ superlattice infrared photodiodes, *Appl. Phys. Lett*. **71**(22), 3251 (1997).

10. P.-Y. Delaunay, B. M. Nguyen, D. Hoffman, E. K.-W. Huang, M. Razeghi, Background Limited Performance of Long Wavelength Infrared Focal Plane Arrays Fabricated From M-Structure InAs–GaSb Superlattices, *IEEE J. Quant. Electron.* **45**(102), 157-162 (2009).

11. H. S. Kim, E. Plis, J. B. Rodriguez, G. D. Bishop, Y. D. Sharma, L. R. Dawson, S. Krishna, J. Bundas, R. Cook, D. Burrows, R. Dennis, K. Patnaude, A. Reisinger, and M. Sundaram, Mid-IR focal plane array based on type-II InAs/GaSb strain layer superlattice detector with nBn design, *Appl. Phys. Lett*. **92**(18), 183502 (2008).

12. C. L. Canedy, E. H. Aifer, I. Vurgaftman, J. G.Tischler, J. R. Meyer, J. H.Warner, E. M. Jackson, Antimonide type-II "W" photodiodes with long-wave infrared R_0A comparable to HgCdTe, *J. Electronic Materials* **36**(8), 852-856 (2007).

13. M. Walther, R. Rehm, J. Fleissner, J. Schmitz, J. Ziegler, W. Cabanski, and R. Breiter, InAs/GaSb type-II short-period superlattices for advanced single and dual-color focal plane arrays, *Proc. SPIE* **6542**, 654206 (2007).

14. C. J. Hill, A. Soibel, S. A. Keo, J. M. Mumolo, S. D. Gunapala, D. R. Rhiger, R. E. Kvaas, and S. F. Harris, Infrared imaging arrays based on superlattice photodiodes, *Proc. SPIE* **6940**, 69400C (2008).

15. H. J. Haugan, F. Szmulowicz, G. J. Brown, and K. Mahalingam, Band gap tuning of InAs/GaSb type-II superlattices for mid-infrared detection, *J. Appl. Phys.* **96**(5), 2580-2585 (2004).

16. B.-M. Nguyen, S. Bogdanov, S. Abdollahi Pour, and M. Razeghi, *Appl. Phys. Lett*. **95**, 183502 (2009).

17. D. Z.-Y. Ting, C. J. Hill, A. Soibel, S. A. Keo, J. M. Mumolo, J. Nguyen, and S. D. Gunapala, A high-performance long wavelength superlattice complementary barrier infrared detector, *Appl. Phys. Lett*. **95**, 023508 (2009).

18. C. J. Hill, A. Soibel, S. A. Keo, J. M. Mumolo, D. Z. Ting, and S.D. Gunapala, Mid-infrared quantum dot barrier photodetectors with extended cutoff wavelengths, *Electronics Letters* **46**(18) 1286-1288 (2010).

19. E. S. Daniel, X. Cartoixa , W. R. Frensley, D. Z.-Y. Ting, and T. C. McGill. "Coupled drift-diffusion/quantum transmitting boundary method simulations of thin oxide devices with specific application to a silicon based tunnel switch diode." *IEEE Trans. Electron Devices* **47**(5), 1052-1060 (2000).

20. David Z. Ting, Alexander Soibel, Jean Nguyen, Linda Höglund, Arezou Khoshakhlagh, Sir B. Rafol, Sam A. Keo, Anna Liao, Jason M. Mumolo, John K. Liu and Sarath D. Gunapala, Type II superlattice barrier infrared detector, Proc. SPIE 8154, 81540L (2011).

21. S. B. Rafol, A. Soibel, A. Khoshakhlagh, J. Nguyen, J. K. Liu, J. M. Mumolo, S. A. Keo, L. Hoeglund D. Z. Ting, and S. D. Gunapala, Performance of a 1/4 VGA Format Long-Wavelength Infrared Antimonides Based Superlattice Focal Plane Array, to appear in J. Quantum Elect. (2012).

22. J.R. Pedrazzani, S. Maimon and G.W. Wicks, "Use of nBn structures to suppress surface leakage currents in unpassivated InAs infrared photodetectors", *Electronics Letters* **44**(25) 1487-U159

23. G. R. Savich, J. R. Pedrazzini, S. Maimon, G. W. Wicks, "Suppression of surface leakage currents using molecular beam epitaxy-grown unipolar barriers", J. Vac. Sci. Technol. B 28(3), C3H18-21 (2010).

24. G. W. Wicks, G. R. Savich, J. R. Pedrazzini, S. Maimon, "Infrared detector epitaxial designs for suppression of surface leakage current", *Proc. of SPIE* **7608**, 760822 (2010).

25. G. R. Savich, J. R. Pedrazzani, D. E. Sidor, S. Maimon, and G. W. Wicks, "Dark current filtering in unipolar barrier infrared detectors", *Appl. Phys. Lett*. **99**, 121112 (2011).

26. G. Bishop, E. Plis, J. B. Rodriguez, Y. D. Sharma, H. S. Kim,L. R. Dawson, and S. Krishna, "nBn detectors based on InAs/GaSb type-II strain layer superlattice", J. Vac. Sci. Technol. B 26(3) 1145 (2008).

Figure Captions:

Figure 1. The energy band diagram of the complementary barrier infrared detector structure with a double tunneling bottom contact, showing the conduction and valence (heavy hole 1) band edges, and the Fermi level (dashed line) under zero bias. The bottom panel shows an enlarged view of the bottom contact region.

Figure 2. The Calculated energy band diagram showing the conduction and valence band edges and the quasi Fermi levels of the CBIRD N-p junction with matching conduction band edges under zero bias (top panel), an N-p junction with a conduction band offset under zero bias (middle panel), and the N-p junction with a conduction band offset under 0.2 V reverse bias (bottom panel).

Figure 3. Top illuminated single-pass spectral responsivity for a CBIRD device without anti-reflection coating under 0.1 V applied bias, measured at 77 K. The inset shows the peak responsivity as a function of applied bias.

Figure 4. Dark current density as a function of applied bias of a 200 μm × 200 μm CBIRD device at 77K operating temperature.

Figure 5. Schematic layer diagram of a quantum-dot barrier infrared detector (QD-BIRD). The absorber region consists of an InAsSb matrix periodically embedded with layers of self-assembled InSb quantum dots.

Figure 6. The top panel shows the photoluminescence (PL) spectrum for the QD-BIRD taken at 77K. The bottom panel shows the double-pass responsivity of a QD-BIRD without anti-reflection coating under -0.2 V applied bias, measured at 125K, 175K, and 225 K.

Figure 7. The inferred schematic energy band diagram for the QD-BIRD absorber near the InSb quantum dots, showing the two transitions responsible for the two peaks observed in the PL spectrum.

Figure 8. Dark current density as a function of applied bias of a 200 μm × 200 μm QD-BIRD taken at 125K, 175K, and 240 K.

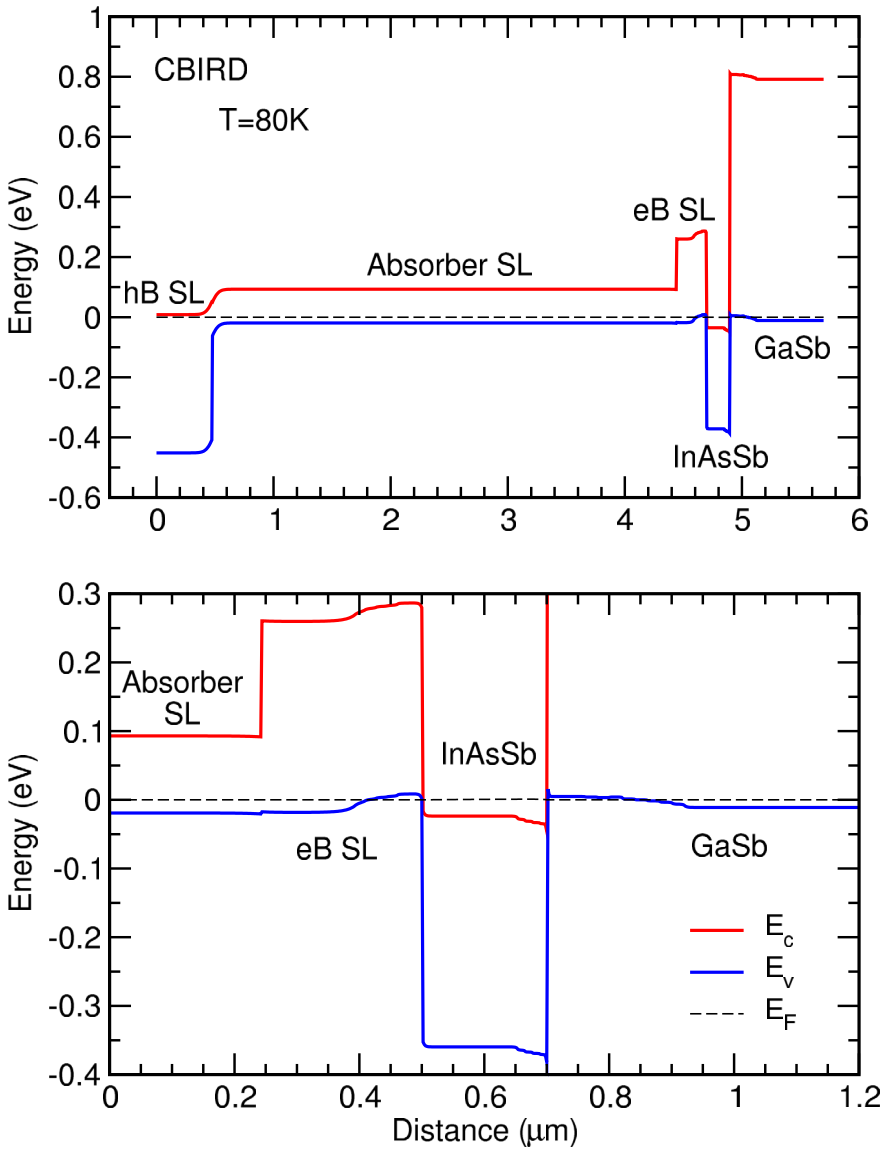

Fig. 1 Ting et al.

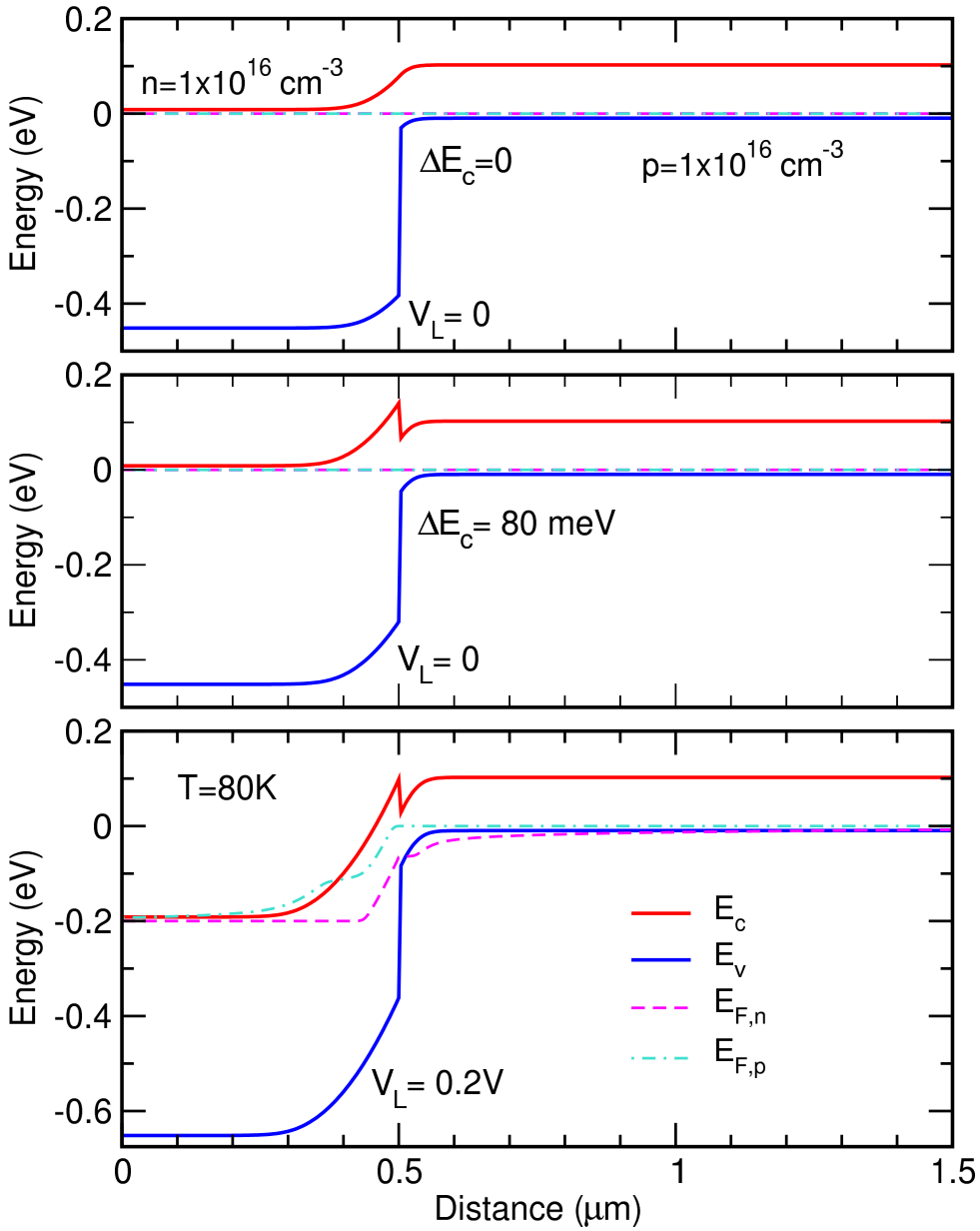

Fig. 2 Ting et al.

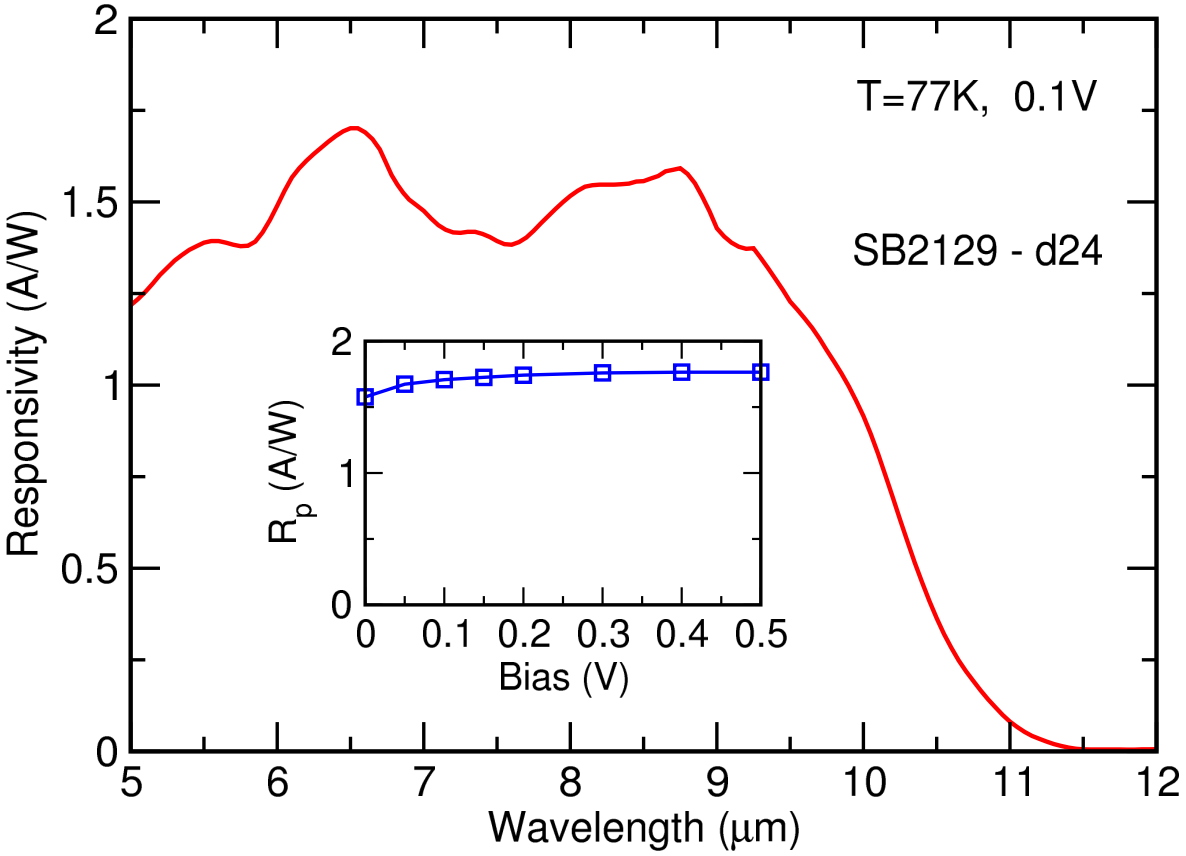

Fig. 3 Ting et al.

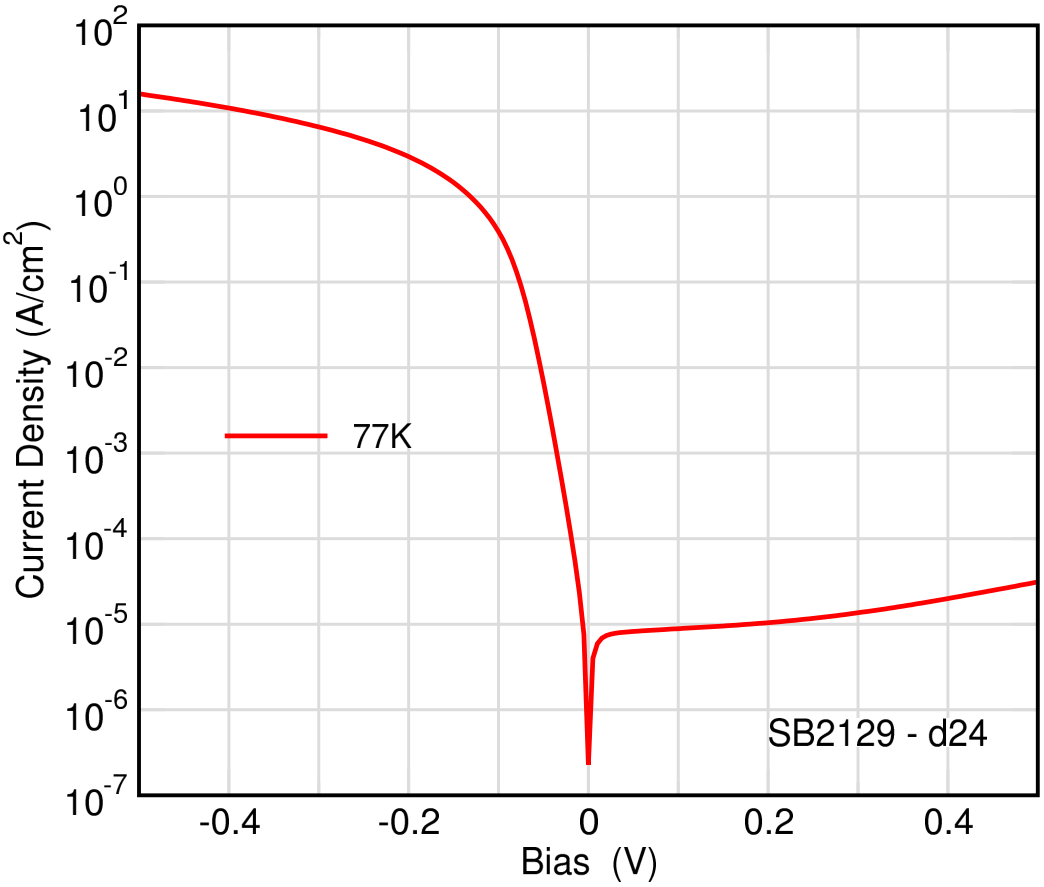

Fig. 4 Ting et al.

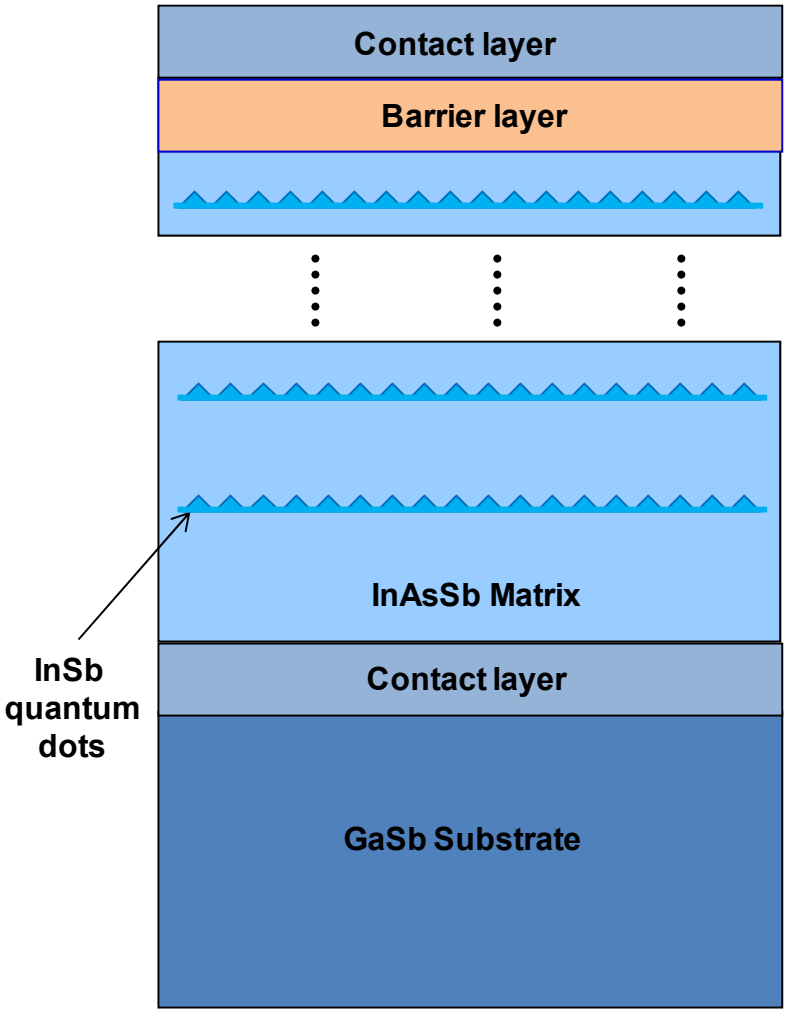

Fig. 5 Ting et al.

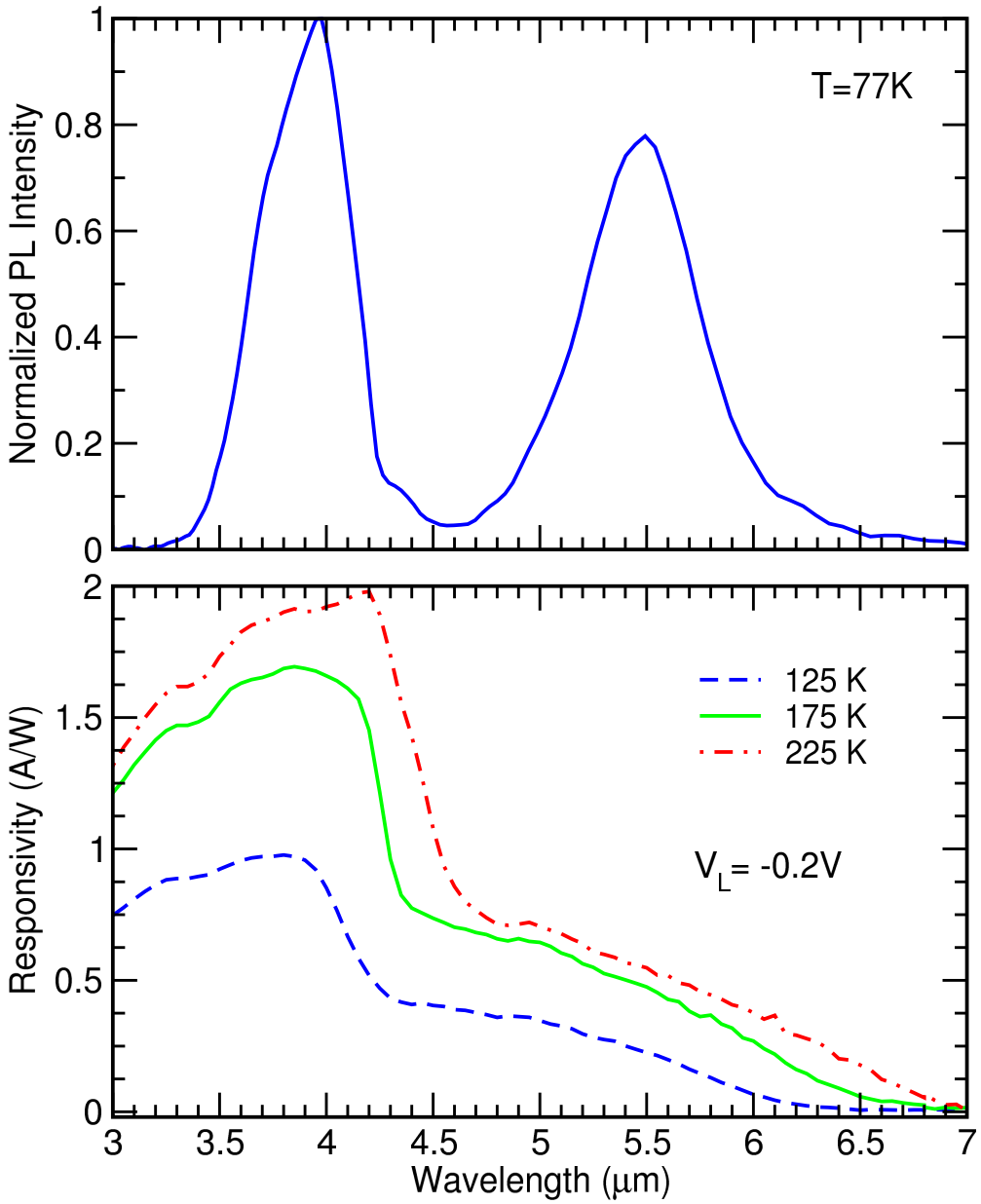

Fig. 6 Ting et al.

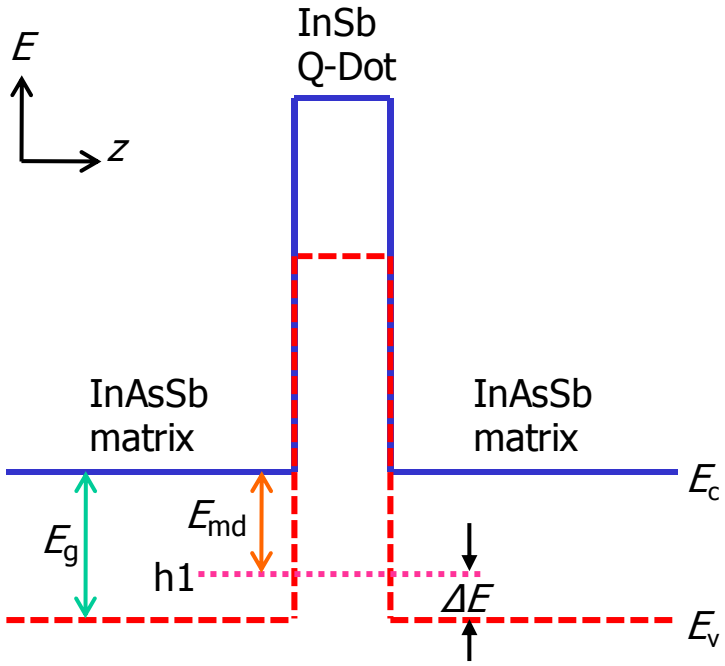

Fig. 7 Ting et al.

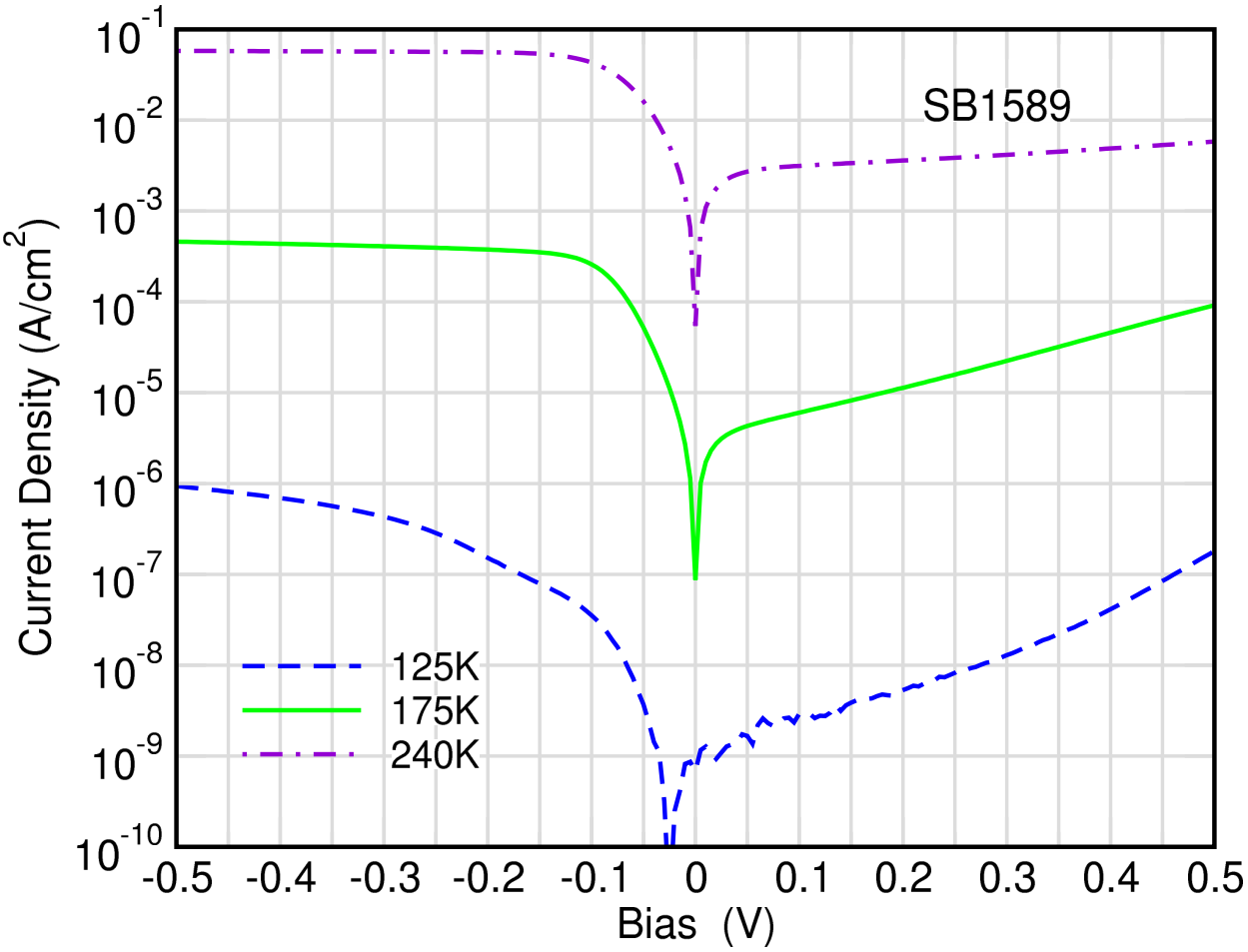

Fig. 8 Ting et al.